

Sequential Joint Shape and Pose Estimation of Vehicles with Application to Automatic Amodal Segmentation Labeling

Josephine Monica¹, Wei-Lun Chao², and Mark Campbell³

Abstract—Shape and pose estimation is a critical perception problem for a self-driving car to fully understand its surrounding environment. One fundamental challenge in solving this problem is the incomplete sensor signal (e.g., LiDAR scans), especially for faraway or occluded objects. In this paper, we propose a novel algorithm to address this challenge, we explicitly leverage the sensor signal captured over consecutive time: the consecutive signals can provide more information of an object, including different viewpoints and its motion. By encoding the consecutive signal via a recurrent neural network, our algorithm not only improves shape and pose estimation, but also produces a labeling tool that can benefit other tasks in autonomous driving research. Specifically, building upon our algorithm, we propose a novel pipeline to automatically annotate high-quality labels for amodal segmentation on images, which are hard and laborious to annotate manually. Our code and data will be made publicly available.

I. INTRODUCTION

A self-driving car must perceive its environment, identify other traffic participants (e.g., vehicles and pedestrians), and importantly, estimate their shapes and poses in order to plan and act safely. One of the fundamental challenges for these problems is the sensor signal: a LiDAR scan may only capture one partial view of an object, making shape and pose estimation an ill-posed problem. Many existing approaches address this challenge using deep learning, training a neural network to encode prior knowledge of complete object shapes [1], [2], [3], [4], [5]. While showing promising results, these approaches are still highly sensitive to the quality of input signals. Specifically, the accuracy of shape and pose estimation drastically drops for faraway objects whose signals are sparse or for occluded objects that are partially observed.

In this paper, we propose to address this challenge by explicitly leveraging consecutive LiDAR scans: we found that most existing methods process each LiDAR scan independently, even though the same object may appear consecutively over time. We argue that consecutive LiDAR scans are crucial for high quality pose and shape estimation. First, while an object may be partially or sparsely observed at each time step, the observations can collectively render a more complete shape over time due to changing viewpoints. Second, traffic participants like vehicles usually move in relatively constrained ways such that temporal information can help correct unreliable pose estimates, as evidenced from

^{1,3}Josephine Monica and Mark Campbell are with the Sibley School of Mechanical and Aerospace Engineering, Cornell University, USA jm2684@cornell.edu, mc288@cornell.edu

²Wei-Lun Chao is with the Department of Computer Science and Engineering, the Ohio State University, USA chao.209@osu.edu

the improvement of video-based object detection [6] and object tracking [7], [8] over frame-wise detection. Third, for an object that is rarely seen in the past (i.e., in the training data), the observation over time essentially offers extra data to adapt the algorithm for improved estimation.

We propose a novel learning-based approach for joint pose and shape estimation that explicitly takes advantage of the consecutive LiDAR scans. Given a sequence of point cloud segments that coarsely captures a single object¹ (specifically, vehicles in this paper), we propose to fuse the newly extracted features from the current point cloud segment with those from the past via a recurrent neural network [18]. Leveraging past measurements provides additional information, especially for estimating the complete shape. In addition, the network can internally learn a motion and behavioral model that is beneficial for pose estimation. We demonstrate that our approach in using consecutive LiDAR scans improves the accuracy of shape and pose estimates through validation on both simulated and real datasets.

Our sequential approach can not only improve shape and pose estimation and its downstream tasks *online*, but also benefit other autonomous driving tasks *offline*. Specifically, for this paper, we propose to apply the approach to automatically annotate labels for preparing data for other tasks. In this paper, we focus on amodal instance segmentation of images, a task aiming to segment the full masks of objects irrespective of potential occlusions among them [19], [20], [21], [22]. This is particularly important in autonomous driving, where dense traffic and adverse conditions (e.g., snow, rain, night) may obfuscate objects. One bottleneck of this research, aside from algorithm design, is the lack of large-scale datasets annotated with ground-truth amodal masks. Concretely, manual annotation of amodal masks is laborious and heavily relies on the subjective intuition of the occluded objects' shape by the annotator, making it hard to maintain consistency and reliability of the labels. Fortunately, most of autonomous driving data are collected in sequence, and usually include both image and LiDAR information. Thus, we leverage the point cloud sequence and our sequential algorithm to estimate the complete 3D object shapes at each time frame, these 3D shape results are then projected onto the corresponding image to obtain the amodal masks. The occlusion ordering can be immediately obtained from depth information. Overall, our *automatic*

¹Point cloud segments of individual objects can be obtained by 3D instance segmentation [9], [10], 3D object detection [11], [12], [13], [14], [15], [16], or clustering [17] in LiDAR point clouds, followed by tracking and associating point cloud segments over time [7], [8].

labeling pipeline helps resolve the ambiguity of manually labeling amodal masks by just looking at just a single image.

Our main contributions are:

- The first joint shape and pose estimation algorithm that leverages information in time frames to improve sequential estimates.
- A simulated dataset of sequences of partial LiDAR measurements of vehicles along with their corresponding complete 3D shapes. The data and data generation code will also be released to enable other researchers to create their own data.
- A novel automatic annotation pipeline for amodal instance segmentation that is built upon our sequential algorithm.

II. RELATED WORK

A. Shape Estimation

Point Completion Network (PCN) [1], one of the pioneers for learning-based shape completion, proposes a simple encoder-decoder shape completion network. [23] designs a new decoder architecture which generates point cloud based on a hierarchical tree structure. More recently, [24] proposes a completion method that directly predicts the missing point cloud and appends it to the point cloud input. However, they all assume well-aligned, canonical point cloud inputs, which are hard to obtain for real sensor data. To operate on real-world data, these methods thus require pose estimation and point cloud alignment to a canonical pose as preprocessing steps. Consequently, the shape estimation is subject to errors from the pose estimation. To address this issue, [4] proposes a network that jointly estimates the pose and complete shape of vehicles, sharing information between the two tasks. Our work builds upon these efforts. However, unlike existing works which make independent estimation for each point cloud input, our method fuses information over time to make more accurate pose and shape estimations.

B. Pose Estimation

Pose estimation in autonomous driving usually refers to inferring the location and orientation of an object. Many detection and tracking algorithms represent vehicles by bounding boxes (parameterized by sizes, orientations, and center locations) and perform traditional filtering, such as the Kalman filter, to fuse new measurements with prior beliefs [25]. However, representing vehicles by bounding boxes eliminate detailed shape information that can facilitate accurate and robust tracking. To make full use of shape information, some trackers [26] apply Iterative Closest Point (ICP) to align point cloud measurements. However, they heavily rely on good initialization and often get stuck in local minimums. As opposed to ICP, Annealed Dynamic Histogram (ADH) tracker [27] globally explores the state space to find the best Markovian alignment between measurements. However, ADH scores the point cloud alignment only based on the latest two measurements. Thus, ADH lacks robustness when the point cloud is sparse or when the viewpoint changes rapidly. Learning-based approaches

[28], [3], [29], [30] benefit from curated training data and can learn to be robust against occlusions and inferior sensor data. However, most of these approaches operate separately on individual frames and do not make use of past information along tracks.

C. Amodal Mask Labeling

Labeling amodal masks is commonly deemed as a subjective and ill-posed problem, as it involves the annotators' intuition to predict the occluded masks. Thus, it requires rigorous guidelines and control to ensure the consistency and quality of the labels. For example, the KINS dataset [31] provides manually annotated amodal mask labels on the autonomous driving KITTI object detection data [32]. To obtain high-quality labels, the data is repetitively labeled six times by three different annotators. This shows the difficulty of amodal mask labeling.

Several attempts have been made to automate the amodal mask label generation. [19] intentionally introduces occlusion to the image by overlaying unoccluded instances with other object masks. The new overlaid image is used as the input data, while the original unoccluded masks serve as the amodal mask label. While this can efficiently provide accurate amodal masks, the generated image may not be realistic or reflect a realistic occlusion relationship in the real world. [33] proposes to align 3D CAD models from PASCAL 3D+ dataset [34] to the target instance in PASCAL VOC [35] images and project the model onto the image frame to acquire the mask. While the generated image comes from a real-world occlusion relationship, the process requires object 3D CAD models and manual alignment of the models.

III. SEQUENTIAL JOINT SHAPE AND POSE ESTIMATION

We formulate the problem of *sequential joint shape and pose estimation* as estimating the homogeneous transformation T_t of an object from the canonical reference pose and its complete point cloud X_t at time t , given unaligned partial point cloud measurements $Z_{1:t}$ of the same object. As vehicles commonly move on a planar ground, we only estimate the planar translation and rotation for T_t . $Z_{1:t}$ can be obtained by a frame-wise point cloud segmentation (e.g., via object detection [11] or instance segmentation [9]), followed by a standard data association over time [37]. Our approach outputs the complete point cloud in the original pose of the unaligned measurement Z_t , rather than in its canonical pose.

A. Pipeline

Our algorithm begins with estimating the pose and complete shape of a vehicle from its first observation using an encoder-decoder-style neural network inspired by [4]. For the sequential time frames, however, unlike existing work, we recursively fuse the newly extracted point cloud features with those from the past through Gated Recurrent Units (GRUs) [18]. Figure 1 shows the overall pipeline of our sequential shape and pose estimation framework. We first preprocess

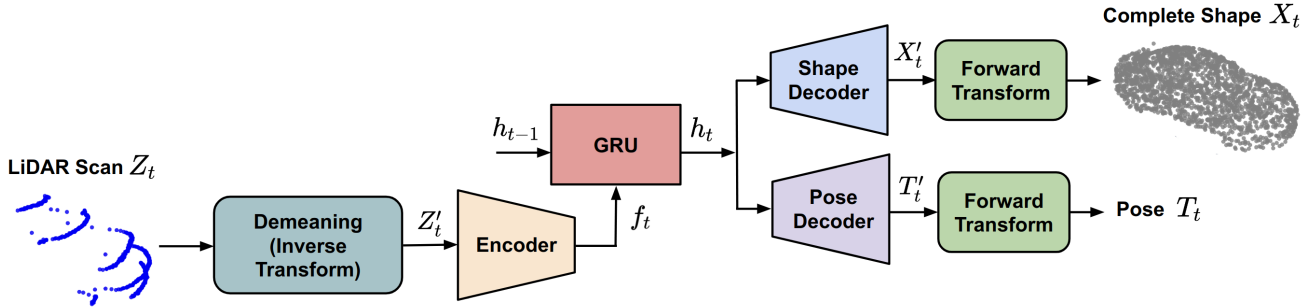


Fig. 1. The overview diagram of our sequential shape and pose estimation pipeline. The point cloud encoder consists of two stacked PointNet [36] layers. The fusion network is a single layer GRU. The shape and pose decoders are Multi-layer Perceptrons (MLPs).

the input by shifting the partial point cloud measurement Z_t by its mean \bar{Z}_t (demeaning in Figure 1):

$$Z'_t = Z_t - \bar{Z}_t \quad (1)$$

In our pipeline, demeaning assists the fusion process by coarsely aligning point cloud measurements from different time steps to the same origin coordinate. Additionally, this step makes training and inference easier by narrowing the network input and output range around the origin. The demeaned point cloud Z'_t is then passed to the joint encoder to extract the feature vector f_t :

$$f_t = f(Z'_t) \quad (2)$$

which summarizes the measurement at time t .

Instead of using f_t alone to generate shape and pose prediction, our method leverages all measurements $Z_{1:t}$ up to the latest frame in making the prediction. In particular, we employ a GRU module [18] which recursively updates its hidden state h_t by fusing the previous hidden state h_{t-1} with the current measurement feature f_t :

$$h_t = \text{GRU}(h_{t-1}, f_t) \quad (3)$$

The hidden state h_t , which can be seen as a summary of all available measurements $Z_{1:t}$, is then used as the input to the pose and shape decoders. This fusion process is executed at the feature level instead of the point-cloud level, allowing the network to better learn how to combine and extract the most useful information from $Z_{1:t}$.

The updated hidden state h_t is then passed to the shape and pose decoders to estimate the complete point cloud X'_t and pose T'_t :

$$X'_t = g_{\text{shape}}(h_t), T'_t = g_{\text{pose}}(h_t) \quad (4)$$

These shape and pose estimates are still in the Z'_t coordinate frame (i.e., coordinate frame whose origin lies at the measurement mean). A forward transformation is applied to bring each back to the original measurement Z_t frame:

$$X_t = X'_t + \bar{Z}_t, T_t = \begin{bmatrix} I & \bar{Z}_t \\ 0 & 1 \end{bmatrix} T'_t \quad (5)$$

Overall, our pipeline shares some conceptual similarities to traditional filtering methods, such as the Kalman filter which

consists of dynamics and measurement update steps. Specifically, our GRU fusion is analogous to the measurement update, and the demeaning block is analogous to the dynamics update in the Kalman filter, but in a reverse manner. Kalman filter updates and transforms the state (e.g., shape and pose) forward in time to the latest measurement coordinate frame. Here instead, we transform the latest measurement back to the previously fused state frame. If we do the dynamics update forward, h_{t-1} must first be decoded to shape and pose before being transformed and encoded again to get the next time step hidden state h_t . This redundant decoding-encoding step induces information loss and produces sub-optimal results. Therefore, we design the dynamics update in reverse.

B. Training

Neural networks that contain multiple components are challenging to train in a naive end-to-end manner. We thus follow [4] to employ a multi-stage training procedure.

Stage 1: We train the encoder, GRU, and shape decoder by minimizing the Chamfer Distance (CD) shape loss [38] between the point cloud estimate X and ground truth X^{gt} :

$$L_{\text{CD}}(X, X^{\text{gt}}) = \frac{1}{|X|} \sum_{\hat{x} \in X} \min_{x \in X^{\text{gt}}} \|\hat{x} - x\|_2 + \frac{1}{|X^{\text{gt}}|} \sum_{x \in X^{\text{gt}}} \min_{\hat{x} \in X} \|x - \hat{x}\|_2 \quad (6)$$

Stage 2: As features from previous shape training have captured some notions about pose [4], we train the pose decoder on top of those features while freezing the rest of the network weights. We train the pose decoder by minimizing the pose loss [39]:

$$L_P(T, T^{\text{gt}}; X^{\text{gt}}) = \frac{1}{|X^{\text{gt}}|} \sum_{x \in X^{\text{gt}}} \|T^{-1}x - (T^{\text{gt}})^{-1}x\|_2^2 \quad (7)$$

where T and T^{gt} are the estimated and ground truth transformations. This loss function penalizes both the translation and rotation errors.

Stage 3: Finally, we jointly train the entire network for sequential shape and pose estimation using the following

joint loss L_J [40]:

$$L_J = \frac{1}{2\sigma_{CD}^2} L_{CD} + \frac{1}{2\sigma_p^2} L_p + \log(\sigma_{CD}\sigma_p) \quad (8)$$

where σ_{CD} and σ_p are learnable parameters, denoting the uncertainty of each prediction task. By training the two tasks simultaneously, learning in one task benefits the other, since the tasks are coupled. Moreover, the network can learn a more general representation capturing both tasks and is less likely to overfit.

IV. AUTOMATIC LABELING FOR AMODAL SEGMENTATION

We extend our sequential algorithm for shape and pose estimation in point clouds to automatic amodal segmentation labeling in images, building on the following key observation. An object instance commonly appears in multiple frames, as driving data is collected in a continuous sequence. Thus, a part of an amodal mask that is occluded in one frame may be visible in other frames. If we can fuse the information from multiple frames, we can produce amodal masks that are consistent across time frames. One naive way is to fuse 2D modal masks in the image space — the 2D masks are easier to annotate or can be obtained from existing segmentation algorithms like Mask-RCNN [41]. This method, however, has several challenges. First, the 2D size of an object can change across frames with respect to the relative pose between the object and camera. Second, the mask shape is also influenced by the object’s 3D orientation, a piece of information that is missing in 2D. Third, while multiple frames provide extra information about an object, some parts of the object may never be seen in all the frames.

To solve these issues, we propose to fuse the information over time in 3D by taking advantage of 1) the 3D LiDAR signal that is commonly available in the autonomous driving configuration, and 2) our learned network for shape completion that encodes the prior of complete shapes from training data. We feed the point cloud sequence into our sequential point completion network in order to obtain the full amodal information of the object. The complete point cloud is then projected to the image space and then post-processed to get the alpha shape as the amodal mask. Finally, the occlusion ordering is reasoned from depth information.

We present two different scenarios where our labeling pipeline can be used. The first assumes the availability of 3D bounding box ground truth and association, which are typically available on a public driving dataset, on the data to be labeled. In this case, the 3D bounding boxes are used to segment the point cloud objects to get a sequence of partial point cloud objects containing only the target vehicle. Given segmented point cloud sequence and ground truth transformations, one can simply accumulate these segmented point clouds using the ground truth transformations and use the symmetrical property of vehicles to mirror the point cloud with respect to its heading direction in order to obtain the amodal shape information. However, this may still result in incomplete amodal information for many cases, as will

be shown in subsection V-C. So instead, we leverage our sequential point completion network to fuse and complete the amodal information. As our goal is labeling, we can train and evaluate the network on the same dataset.

In the second scenario, we handle the situation where 3D bounding box labels are not available. In this case, we deploy a pretrained Mask-RCNN [41] inmodal instance segmentation and LDLS [9] (a 2D to 3D label diffusion framework) to segment the point cloud, followed by data association. Since 3D bounding box labels are not available, we deploy our sequential completion network that is pretrained on other dataset, e.g., synthetic dataset.

V. EXPERIMENTS

We first evaluate the quality of the completed point cloud and pose estimates on the synthetic and Argoverse [42] real dataset. The translation and rotation errors are computed to evaluate the pose estimate quality. Besides Chamfer Distance (CD), Earth Mover Distance (EMD) [39], [43] is also computed to evaluate the completed point cloud through different aspects. The CD captures the global structure of the point cloud, while the EMD captures the point density.

Next, we evaluate our automatic amodal labeling pipeline on the KITTI tracking dataset, comparing our generated masks to the manually annotated labels from KINS by computing the mean intersection over union (mIoU), as well as % miss, i.e., the percentage of instances that do not have a matching or $\text{IoU} < 0.5$.

A. Data Generation

The synthetic dataset can generate perfect and complete point clouds required for training and evaluation. However, the synthetic dataset does not contain real-world challenges such as occlusions, contamination from ground points, LiDAR time synchronization issues, and data mislabeling. Thus, we complement our analysis by training and evaluating on the real-world Argoverse dataset [42].

1) *Synthetic Dataset*: We obtain 183 vehicle CAD models from [44] and randomly split them to 168/15 for training and validation. Each CAD model is fit into 11 different trajectories, where each may contain a different number of frames, resulting in 1848/165 tracks for training and validation. To mimic the real-world behavior of vehicles, we use the trajectory log from the Argoverse dataset [42].

To simulate partial point cloud measurements, we transform the CAD models to the desired pose in the track and apply raytracing using the Trimesh library [45]. We generate synthetic with the configuration of VLP-16 LiDAR that is placed at a 2m height from the ground. To generate a complete point cloud shape, we use Open3D library [46] to sample points from the CAD models and remove interior points that are not visible from the outside.

2) *Argoverse*: We evaluate our results on vehicle objects in the Argoverse tracking dataset [42] split into 2298 tracks for training and 638 tracks for validation, where each track contains an average of 70 frames. As we do not focus on the problem of segmentation and data association, ground truth

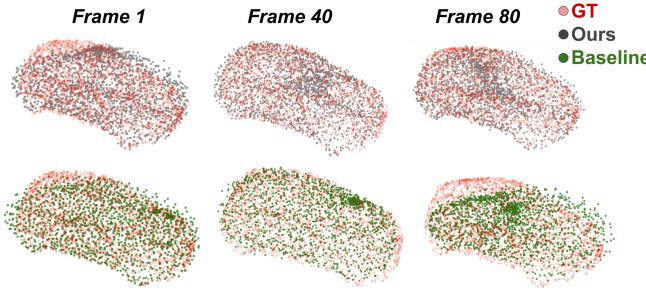


Fig. 2. Qualitative shape completion results on a track from the synthetic data over time. Top: Ours. Bottom: Baseline.

bounding boxes and track ids are used to crop the LiDAR scene.

While ground truth pose is provided by Argoverse, complete point clouds are not available. Thus, to acquire a shape reference, LiDAR point clouds of vehicles are accumulated over multiple frames. Furthermore, since vehicles are usually symmetrical about their heading axis, we mirror the points along the symmetrical heading axis [47]. Note that even after the LiDAR point clouds are accumulated and mirrored, there still may be errors in the developed shape reference, including noise, inaccuracy, incompleteness and non uniform point density, as they are built from measurements. As these properties are highly crucial for EMD, evaluating EMD against such point cloud reference is not meaningful. Thus, we do not report the EMD for Argoverse evaluation.

B. Shape and Pose Estimation

We run our method recursively from each vehicle’s initial to final detection. The shape and pose errors are evaluated at each time step. We compare our method to the joint shape and pose estimation from [4] as a baseline. Different from our proposed approach, the baseline makes a prediction on each frame independently.

1) *Results on Synthetic Dataset*: Table I shows the sequential shape and pose estimation results on the synthetic dataset. Our method outperforms the baseline in both shape completion and pose estimation tasks. While the CD is the direct metric for training, EMD quantifies the quality of point density. The reported EMD value is much higher than CD due to requiring one-to-one correspondences between points. Nevertheless, our method still outperforms the baseline even on EMD metric.

TABLE I

QUANTITATIVE RESULT ON THE SYNTHETIC DATASET.

Method	Shape Error		Pose Error	
	CD	EMD	Translation	Rotation
Baseline	3.1 cm	0.50 m	12.2 cm	20.2°
Ours	2.3 cm	0.25 m	9.4 cm	12.0°

To complement the quantitative analysis, shape estimate results at three different time instances are shown in Figure 2.

In this case, the sensor data is initially (frame 1) very sparse. Both methods do not produce accurate shape estimates; they also mispredict the orientation of the car by roughly 180°. At frame 40, the sensor data is denser, and both methods produce more accurate shape estimates. Nevertheless, we can still observe that our shape estimate fits the ground truth better. At frame 80, the sensor data becomes sparse again. As a result, the baseline approach produces an inaccurate shape estimate and a large orientation error, as can be seen from Figure 2. Yet, at this time, our method produces an accurate shape estimate despite the challenging sensor measurement. This shows that by leveraging temporal information, we can produce more accurate and consistent estimates over time.

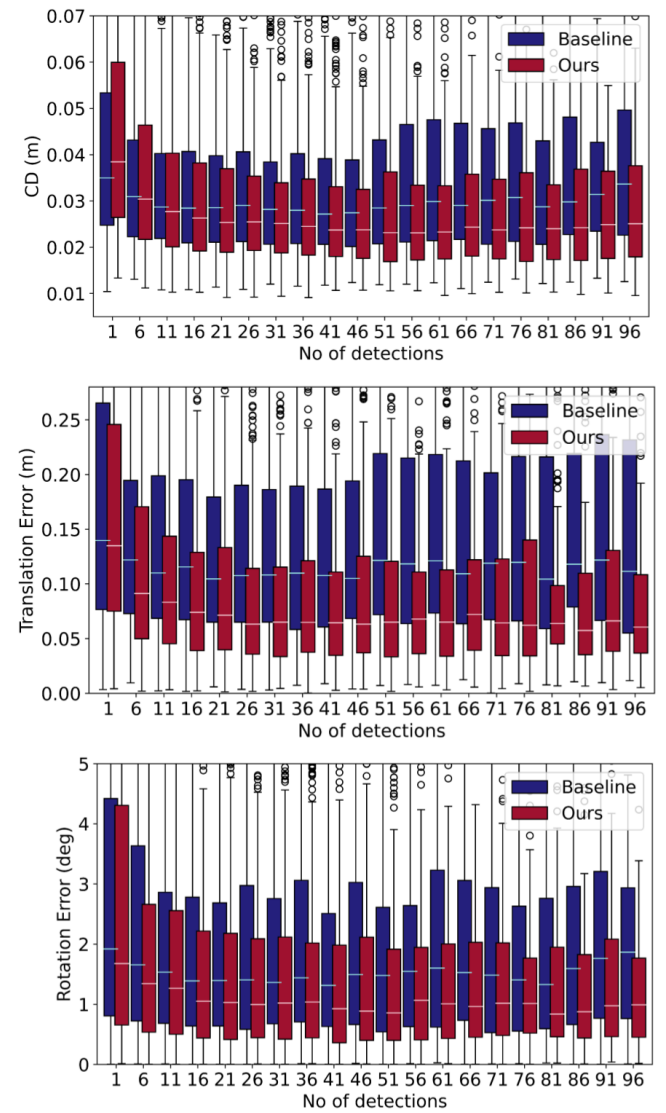


Fig. 3. Statistical analysis on the shape and pose accuracy as a function of number of detections on the Argoverse dataset. Top: CD metric. Mid: Translational error. Bottom: Rotational error. Lower is better.

2) *Results on Argoverse Dataset*: Figure 3 plots the shape and pose estimate error metrics with respect to the number of detections. Our method outperforms the baseline in all metrics and shows a general trend of improvement in the

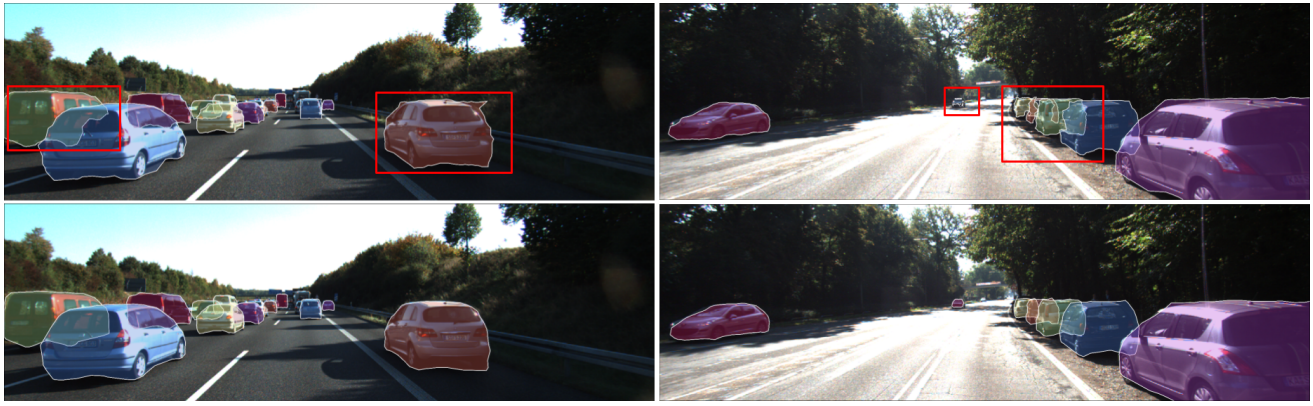


Fig. 4. Annotated amodal masks from our proposed pipelines. Top: GT-Accumulation. Bottom: GT-SC. The masks inside the red boxes highlight the benefit of using our sequential completion network.

quality of shape estimates with more detections. This aligns with our initial claim that performance improves with more frames if fused properly.

C. Automatic Labeling of Amodal Segmentation on KITTI

Table II shows the result of our automatic amodal labeling pipeline compared to KINS. KINS-manual mIoU represents the consistency of their manually annotated labels across different annotators. GT-Accumulation method refers to accumulating and mirroring partial point cloud sequence. SC-GT refers to sequential completion with ground truth bounding boxes. SC-MRCNN refers to sequential completion using Mask-RCNN [41] and label diffusion when 3D ground truth bounding boxes are unavailable. In all cases (with and without 3D bounding box labels), our proposed labeling approach achieves comparable mIoU consistency to human-level performance, i.e., KINS cross annotators consistency. In the case where 3D ground truth bounding boxes are available, running through sequential completion (SC-GT) yields less missing instance match than just accumulating and mirroring (GT-Accumulation). Importantly, we compare our generated masks to the manually annotated KINS label and not to the actual amodal mask ground truth that is practically unavailable. The KINS label itself has some noise, i.e., its internal consistency across different annotators is ~ 0.8 . Thus, achieving a higher mIoU than that does not necessarily imply a better quality mask.

TABLE II
AMODAL MASK CONSISTENCY.

Method	3D GT label	% Miss	mIoU
KINS-manual	-	-	0.809
GT-Accumulation	Available	2.69	0.813
SC-GT	Available	0.90	0.813
SC-MRCNN	No	5.53	0.788

Thus, to give a better insight into the advantage of our sequential completion network, we qualitatively show several amodal mask examples in Figure 4. Specifically, note the area

inside the red boxes. We observe cases where merely accumulating and mirroring (GT-Accumulation) is not enough to cover the full amodal information. Additionally, GT-Accumulation is prone to error or noise in the point cloud, as shown in the white car inside the red box in Figure 4 top left. On the other hand, despite the noise, our sequential completion network has a smoothing effect that filters out this noise.

Finally, in the absence of 3D ground truth bounding boxes, we can not perform our accumulation and mirroring method (GT-Accumulation). But our sequential completion network (SC-MRCNN) still provides comparable quality masks to human-annotated labels despite the absence of any labels. Although as expected, the performance of SC-MRCNN is slightly worse than SC-GT. This is because segmenting out point cloud using Mask-RCNN and LDLS is not as accurate as using human-annotated 3D ground truth bounding boxes. Additionally, due to the absence of 3D ground truth bounding boxes, the sequential completion network in SC-MRCNN is trained on the synthetic data, which introduces some domain adaptation gap when applied to the KITTI data.

VI. CONCLUSION

We propose a learning-based approach for joint point completion and pose estimation of vehicles from LiDAR point cloud measurements. Uniquely, our method explicitly leverages the temporal information of tracks. We evaluate our method on synthetic and real-world datasets, showing better performance in both shape and pose estimation tasks against the baseline approach. Additionally, we demonstrate that properly fusing extra temporal information benefits shape and pose estimation. Using our sequential completion network, we propose a novel automatic amodal labeling pipeline. We evaluate our automatic amodal labeling pipeline and demonstrate comparable quality to human annotations.

ACKNOWLEDGEMENT

The authors would like to acknowledge the support from NSF grant S&AS: INT: Inference, Reasoning and Learning for Robust Autonomous Driving Grant, IIS-1724282.

REFERENCES

[1] Wentao Yuan, Tejas Khot, David Held, Christoph Mertz, and Martial Hebert. PCN: point completion network. *CoRR*, abs/1808.00671, 2018.

[2] Xiaogang Wang, Marcelo H Ang Jr, and Gim Hee Lee. Point cloud completion by learning shape priors. *arXiv preprint arXiv:2008.00394*, 2020.

[3] Wentao Yuan, David Held, Christoph Mertz, and Martial Hebert. Iterative transformer network for 3d point cloud. *arXiv preprint arXiv:1811.11209*, 2018.

[4] Hunter Goforth, Xiaoyan Hu, Michael Happold, and Simon Lucey. Joint pose and shape estimation of vehicles from lidar data. *arXiv preprint arXiv:2009.03964*, 2020.

[5] Jiayuan Gu, Wei-Chiu Ma, Sivabalan Manivasagam, Wenyuan Zeng, Zihao Wang, Yuwen Xiong, Hao Su, and Raquel Urtasun. Weakly-supervised 3d shape completion in the wild. In *Proc. of the European Conf. on Computer Vision (ECCV)*. Springer, 2020.

[6] Junbo Yin, Jianbing Shen, Chenye Guan, Dingfu Zhou, and Ruigang Yang. Lidar-based online 3d video object detection with graph-based message passing and spatiotemporal transformer attention. In *CVPR*, 2020.

[7] Xinshuo Weng and Kris Kitani. A baseline for 3d multi-object tracking. *arXiv preprint arXiv:1907.03961*, 2019.

[8] Tianwei Yin, Xingyi Zhou, and Philipp Krähenbühl. Center-based 3d object detection and tracking. *arXiv preprint arXiv:2006.11275*, 2020.

[9] Brian H Wang, Wei-Lun Chao, Yan Wang, Bharath Hariharan, Kilian Q Weinberger, and Mark Campbell. Ldls: 3-d object segmentation through label diffusion from 2-d images. *IEEE Robotics and Automation Letters*, 4(3):2902–2909, 2019.

[10] Bichen Wu, Alvin Wan, Xiangyu Yue, and Kurt Keutzer. Squeezeseg: Convolutional neural nets with recurrent crf for real-time road-object segmentation from 3d lidar point cloud. In *2018 IEEE International Conference on Robotics and Automation (ICRA)*, pages 1887–1893. IEEE, 2018.

[11] Shaoshuai Shi, Xiaogang Wang, and Hongsheng Li. Pointrcnn: 3d object proposal generation and detection from point cloud. In *CVPR*, 2019.

[12] Yan Wang, Wei-Lun Chao, Divyansh Garg, Bharath Hariharan, Mark Campbell, and Kilian Q. Weinberger. Pseudo-lidar from visual depth estimation: Bridging the gap in 3d object detection for autonomous driving. In *CVPR*, 2019.

[13] Yurong You, Yan Wang, Wei-Lun Chao, Divyansh Garg, Geoff Pleiss, Bharath Hariharan, Mark Campbell, and Kilian Q. Weinberger. Pseudo-lidar++: Accurate depth for 3d object detection in autonomous driving. In *ICLR*, 2020.

[14] Charles R Qi, Wei Liu, Chenxia Wu, Hao Su, and Leonidas J Guibas. Frustum pointnets for 3d object detection from rgb-d data. In *CVPR*, 2018.

[15] Alex H Lang, Sourabh Vora, Holger Caesar, Lubing Zhou, Jiong Yang, and Oscar Beijbom. Pointpillars: Fast encoders for object detection from point clouds. In *ICCV*, pages 12697–12705, 2019.

[16] Yin Zhou and Oncel Tuzel. Voxelenet: End-to-end learning for point cloud based 3d object detection. In *CVPR*, 2018.

[17] Erich Schubert, Jörg Sander, Martin Ester, Hans Peter Kriegel, and Xiaowei Xu. Dbscan revisited, revisited: why and how you should (still) use dbscan. *ACM Transactions on Database Systems (TODS)*, 42(3):1–21, 2017.

[18] Junyoung Chung, Caglar Gulcehre, KyungHyun Cho, and Yoshua Bengio. Empirical evaluation of gated recurrent neural networks on sequence modeling. *arXiv preprint arXiv:1412.3555*, 2014.

[19] Ke Li and Jitendra Malik. Amodal instance segmentation. In *European Conference on Computer Vision*, pages 677–693. Springer, 2016.

[20] Yan Zhu, Yuandong Tian, Dimitris Metaxas, and Piotr Dollár. Semantic amodal segmentation. In *Proceedings of the IEEE conference on computer vision and pattern recognition*, pages 1464–1472, 2017.

[21] Yuting Xiao, Yanyu Xu, Ziming Zhong, Weixin Luo, Jiawei Li, and Shenghua Gao. Amodal segmentation based on visible region segmentation and shape prior. *arXiv preprint arXiv:2012.05598*, 2020.

[22] Xiaohang Zhan, Xingang Pan, Bo Dai, Ziwei Liu, Dahua Lin, and Chen Change Loy. Self-supervised scene de-occlusion. In *Proceedings of the IEEE/CVF Conference on Computer Vision and Pattern Recognition*, pages 3784–3792, 2020.

[23] Lyne P Tchapmi, Vineet Kosaraju, Hamid Rezatofighi, Ian Reid, and Silvio Savarese. Topnet: Structural point cloud decoder. In *Proceedings of the IEEE/CVF Conference on Computer Vision and Pattern Recognition*, pages 383–392, 2019.

[24] Zitian Huang, Yikuan Yu, Jiawen Xu, Feng Ni, and Xinyi Le. Pf-net: Point fractal network for 3d point cloud completion. In *Proceedings of the IEEE/CVF Conference on Computer Vision and Pattern Recognition*, pages 7662–7670, 2020.

[25] Xinshuo Weng and Kris Kitani. A baseline for 3d multi-object tracking. *CoRR*, abs/1907.03961, 2019.

[26] Adam Feldman, Maria Hybinette, and Tucker Balch. The multi-iterative closest point tracker: An online algorithm for tracking multiple interacting targets. *Journal of Field Robotics*, 29(2):258–276, 2012.

[27] David Held, Jesse Levinson, Sebastian Thrun, and Silvio Savarese. Robust real-time tracking combining 3d shape, color, and motion. *The International Journal of Robotics Research*, 35(1-3):30–49, 2016.

[28] Johannes Groß, Aljosa Osep, and Bastian Leibe. Alignnet-3d: Fast point cloud registration of partially observed objects. *CoRR*, abs/1910.04668, 2019.

[29] Wentao Yuan, Benjamin Eckart, Kihwan Kim, Varun Jampani, Dieter Fox, and Jan Kautz. Deepgmr: Learning latent gaussian mixture models for registration. In *European Conference on Computer Vision*, pages 733–750. Springer, 2020.

[30] Frederik Hagelskjær and Anders Glent Buch. Pointvotenet: Accurate object detection and 6 dof pose estimation in point clouds. In *2020 IEEE International Conference on Image Processing (ICIP)*, pages 2641–2645. IEEE, 2020.

[31] Lu Qi, Li Jiang, Shu Liu, Xiaoyong Shen, and Jiaya Jia. Amodal instance segmentation with kins dataset. In *Proceedings of the IEEE/CVF Conference on Computer Vision and Pattern Recognition*, pages 3014–3023, 2019.

[32] Andreas Geiger, Philip Lenz, Christoph Stiller, and Raquel Urtasun. Vision meets robotics: The kitti dataset. *The International Journal of Robotics Research*, 32(11):1231–1237, 2013.

[33] Abhishek Kar, Shubham Tulsiani, Joao Carreira, and Jitendra Malik. Amodal completion and size constancy in natural scenes. In *Proceedings of the IEEE International Conference on Computer Vision*, pages 127–135, 2015.

[34] Yu Xiang, Roozbeh Mottaghi, and Silvio Savarese. Beyond pascal: A benchmark for 3d object detection in the wild. In *IEEE winter conference on applications of computer vision*, pages 75–82. IEEE, 2014.

[35] Mark Everingham and John Winn. The pascal visual object classes challenge 2012 (voc2012) development kit. *Pattern Analysis, Statistical Modelling and Computational Learning, Tech. Rep.*, 8:5, 2011.

[36] Charles Ruizhongtai Qi, Hao Su, Kaichun Mo, and Leonidas J. Guibas. Pointnet: Deep learning on point sets for 3d classification and segmentation. *CoRR*, abs/1612.00593, 2016.

[37] Dirk Schulz, Wolfram Burgard, Dieter Fox, and Armin B Cremers. Tracking multiple moving targets with a mobile robot using particle filters and statistical data association. In *Proceedings 2001 ICRA. IEEE International Conference on Robotics and Automation (Cat. No. 01CH37164)*, volume 2, pages 1665–1670. IEEE, 2001.

[38] Haoqiang Fan, Hao Su, and Leonidas J. Guibas. A point set generation network for 3d object reconstruction from a single image. *CoRR*, abs/1612.00603, 2016.

[39] Stefan Hinterstoisser, Vincent Lepetit, Slobodan Ilic, Stefan Holzer, Gary Bradski, Kurt Konolige, and Nassir Navab. Model based training, detection and pose estimation of texture-less 3d objects in heavily cluttered scenes. In *Asian conference on computer vision*, pages 548–562. Springer, 2012.

[40] Alex Kendall, Yarin Gal, and Roberto Cipolla. Multi-task learning using uncertainty to weigh losses for scene geometry and semantics. In *Proceedings of the IEEE conference on computer vision and pattern recognition*, pages 7482–7491, 2018.

[41] Kaiming He, Georgia Gkioxari, Piotr Dollár, and Ross Girshick. Mask r-cnn. In *ICCV*, 2017.

[42] Ming-Fang Chang, John Lambert, Patsorn Sangkloy, Jagjeet Singh, Slawomir Bak, Andrew Hartnett, De Wang, Peter Carr, Simon Lucey, Deva Ramanan, and James Hays. Argoverse: 3d tracking and forecasting with rich maps. *CoRR*, abs/1911.02620, 2019.

[43] Minghua Liu, Lu Sheng, Sheng Yang, Jing Shao, and Shi-Min Hu. Morphing and sampling network for dense point cloud completion. *arXiv preprint arXiv:1912.00280*, 2019.

[44] Sanja Fidler, Sven Dickinson, and Raquel Urtasun. 3d object detection and viewpoint estimation with a deformable 3d cuboid model. In *NIPS*, 2012.

- [45] Dawson-Haggerty et al. trimesh. <https://trimsh.org/>, 2019. version: 3.2.0.
- [46] Qian-Yi Zhou, Jaesik Park, and Vladlen Koltun. Open3D: A modern library for 3D data processing. *arXiv:1801.09847*, 2018.
- [47] Sivabalan Manivasagam, Shenlong Wang, Kelvin Wong, Wenyuan Zeng, Mikita Sazanovich, Shuhan Tan, Bin Yang, Wei-Chiu Ma, and Raquel Urtasun. Lidarsim: Realistic lidar simulation by leveraging the real world. In *Proceedings of the IEEE/CVF Conference on Computer Vision and Pattern Recognition*, pages 11167–11176, 2020.